Robust Two-Qubit Gates for Trapped Ions Using Spin-Dependent Squeezing

Yotam Shapira,[1] Sapir Cohen,[2] Nitzan Akerman,[1] Ady Stern,[2] and Roee Ozeri[1]
[1]Department of Physics of Complex Systems, Weizmann Institute of Science, Rehovot 7610001, Israel
[2]Department of Condensed Matter Physics, Weizmann Institute of Science, Rehovot 7610001, Israel

(Received 6 July 2022; accepted 7 December 2022; published 20 January 2023)

Entangling gates are an essential component of quantum computers. However, generating high-fidelity gates, in a scalable manner, remains a major challenge in all quantum information processing platforms. Accordingly, improving the fidelity and robustness of these gates has been a research focus in recent years. In trapped ions quantum computers, entangling gates are performed by driving the normal modes of motion of the ion chain, generating a spin-dependent force. Even though there has been significant progress in increasing the robustness and modularity of these gates, they are still sensitive to noise in the intensity of the driving field. Here we supplement the conventional spin-dependent displacement with spin-dependent squeezing, which creates a new interaction, that enables a gate that is robust to deviations in the amplitude of the driving field. We solve the general Hamiltonian and engineer its spectrum analytically. We also endow our gate with other, more conventional, robustness properties, making it resilient to many practical sources of noise and inaccuracies.

DOI: 10.1103/PhysRevLett.130.030602

Two-qubit entanglement gates are a crucial component of quantum computing, as they are an essential part of a universal gate set. Moreover, fault-tolerant quantum computing requires gates with fidelities above the fault-tolerance threshold [1]. Generating high-fidelity two-qubit gates in a robust and scalable manner remains an open challenge, and a research focus, in all current quantum computing platforms [2–4].

Trapped ions based quantum computers are a leading quantum computation platform, due to their high controllability, long coherence times, and all-to-all qubit connectivity [5–7]. Entanglement gates are typically generated by driving the ions with electromagnetic fields that create phonon mediated qubit-qubit interactions. Such gates have been demonstrated, with outstanding fidelities [8–11]. Moreover, in recent years there have been many theoretical proposals and experimental demonstrations [12–43] aimed at improving the fidelity, rate, connectability, and resilience of such gates. These schemes are largely based on generating spin-dependent displacement forces on the ions which, depending on realization, are linear or quadratic in the driving field. These result in gates which are sensitive to the field amplitude and exhibit a degradation of fidelity which is linear in field intensity noise. A widely used scheme for which is the Mølmer-Sørensen (MS) gate [44,45]. Driving field amplitude deviations arise naturally in trapped ions systems and may come about due to intensity noise in the drive source, as well as beam pointing noise and polarization noise [46,47].

Here we propose a gate scheme which is resilient to deviations in the driving field's amplitude. We combine the conventional spin-dependent displacement with spin-dependent squeezing, by driving the first and second motional sidebands of the ion crystal normal modes. We solve the resulting interaction analytically and formulate constraints on the drive which generate a resilient gate. Crucially, most constraints can be easily satisfied without any numerical optimization. We combine other well-known robustness methods, resulting in a two-qubit entanglement gate which is resilient to many experimental parameters and is independent of the initial motional state, within the Lamb-Dicke regime. Our gates may be implemented using conventional waveform spectral shaping which is straightforward to implement and is common to trapped ions systems. Our method is compatible to laser driven gates as well as laser-free entangling gates [11].

While we make use of the combination of spin-dependent displacement and spin-dependent squeezing for increasing the gate robustness, our derivations promote the utilization of this combination to other aspects of trapped ions quantum computing as well, such as improved fidelity, programmability, and gate rate.

Figure 1 showcases our main results, with the fidelity (left) of our gate (blue line) and the conventional MS gate (red line), in the presence of deviations in the field's Rabi frequency $\delta\Omega$. As seen, our gate shows a robust response which scales as $\delta\Omega^4$, and exhibits a high-fidelity entangling operation even with 10% Rabi frqeuency errors. This is contrasted by the quadratic error of a MS gate. The population dynamics of the initial state $|00\rangle$ are shown (right) for the ideal, $\delta\Omega = 0$, case (solid lines) and in the presence of a deviation, with $\delta\Omega/\Omega = 0.05$ (dashed lines). While the two cases exhibit different dynamics, at the gate

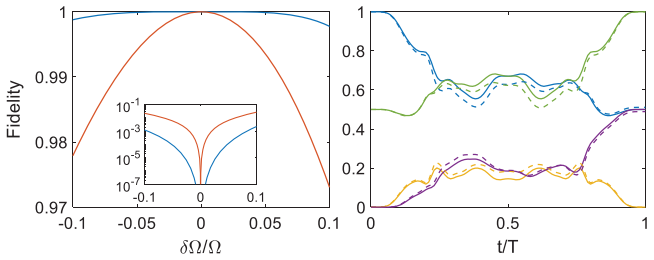

FIG. 1. Robust gate performance. Left: fidelity of our robust gate (blue lines) and the conventional MS gate (red lines), in presence of a deviation of the laser's Rabi frequency $\delta\Omega$. Our gate shows a flat response, that scales as $\delta\Omega^4$, yielding a high-fidelity operation even in the presence of 10% errors. The MS gate exhibits a quadratic response and a fast deterioration in fidelity. The inset shows the infidelity, $1-F$, in log scale. Our method typically provides more than 2 orders of magnitude of improvement throughout the 10% error range. Right: population dynamics of the initial state $|00\rangle$, for an ideal case (solid lines) and an erroneous case, with a 5% Rabi frequency error (dashed lines). In both cases a high-fidelity operation (green lines) is generated at the gate time $t=T$, indicated by an equal population of the $|00\rangle$ (blue lines) and $|11\rangle$ (purple lines) states, while the $|01\rangle$ and $|10\rangle$ populations (orange lines) vanish, indicating robustness to Rabi frequency deviations.

time $t=T$ they both converge and result in a high-fidelity Bell state (green lines).

Utilizing spin-dependent squeezing for entangling gates has been suggested in other contexts, such as in order to generate gates in the strong-coupling regime [33], or in order to generate three-body [48] and n-body [49] interaction terms.

Below we present the Hamiltonian of interest, its solution, the formulation of constraints, and their resolution using spectral shaping. Finally, we analyze our gate's performance and feasibility.

We start with the noninteracting Hamiltonian of two trapped ions, given by ($\hbar=1$),

$$H_0=\omega_0 J_z+\nu a^\dagger a, \tag{1}$$

with ω_0 the single ion separation frequency of the relevant qubit levels, $J_z=(\sigma_1^z+\sigma_2^z)/2$ the global Pauli-z operator such that σ_n^z is the z-Pauli operator acting on the nth ion, and ν the frequency of a normal mode of motion of the ion chain, equally coupled to the two ions, and its phonon creation operator $a^\dagger$. All other modes of motion are assumed to be decoupled from the ion's evolution, yet this assumption can be relaxed [27]. The Hamiltonian in Eq. (1) can trivially be used in a larger ion chain, by assuming only two ions are illuminated [41,50].

Without loss of generality and for concreteness we assume the ion qubit levels are coupled by a direct optical transition. The ions are driven by a multitone global laser field with a spectral content in the vicinity of the first and second motional sidebands. This yields the interaction Hamiltonian,

$$V_I=J_x[w_1(t)a^\dagger+iw_2(t)(a^\dagger)^2]+\text{H.c.}, \tag{2}$$

with $w_n(t)=\sum_m \rho_{n,m}e^{i\delta_{n,m}t}$. Here $\rho_{n,m}$ and $\delta_{n,m}$ are amplitudes and frequencies determined below. Equation (2) is obtained in a frame rotating with respect to H_0, and by driving the ion chain with the global time-dependent drive,

$$W(t)=-\frac{4}{\eta}\sin(\omega_0 t)\sum_m \rho_{1,m}\cos[(\nu-\delta_{1,m})t] -\frac{8}{\eta^2}\cos(\omega_0 t)\sum_m \rho_{2,m}\sin[(2\nu-\delta_{2,m})t], \tag{3}$$

with η the Lamb-Dicke parameter, quantifying the coupling between qubit and motional states [51]. The structure of Eq. (3) implies that the w_n's are proportional to Ω, the driving field's Rabi frequency. The resulting interaction in Eq. (2) is valid in terms of a rotating wave approximation (RWA) in Ω/ω_0 and a second order expansion in η. Furthermore, we make use of a RWA in Ω/ν allowing us to omit off-resonance carrier coupling terms and counterrotating terms. Below we incorporate methods that eliminate carrier coupling terms even further [18]. We note that counterrotating terms still allow for an analytic solution [27], but are omitted here in favor of a more concise presentation. Note that the $w_n(t)$'s can be arbitrary complex time-dependent functions.

For the oscillator, the Hamiltonian in Eq. (2) generates both a spin-dependent displacing term, modulated by w_1, and a spin-dependent squeezing term, modulated by w_2. In the special case of $w_2=0$ the interaction V_I reduces to the MS Hamiltonian and is exactly solvable. We show below that we may still solve it for nonvanishing second sideband modulations.

There exists a known solution to general time-dependent quantum harmonic oscillators [52]. However, here the appearance of spin dependence requires special care. We move to a frame rotating with respect to a spin-dependent squeezing by applying a unitary transformation, $S(J_x r)=\exp\{(J_x r/2)[a^2-(a^\dagger)^2]\}$, with the time-dependent parameter $r(t)$, for which we assume $r(t=0)=0$. This transforms V_I to $V_S=S^\dagger V_I S-iS^\dagger\partial_t S$ (see the Supplemental Material [53]). Choosing $w_2\in\mathbb{R}$, i.e., the spectrum of w_2 is symmetric around the second sideband, the term in V_S that is proportional to $J_x a^2$ is

$$V_S^{(J_x a^2)}=-iJ_x a^2\left(w_2+\frac{1}{2}\partial_t r\right). \tag{4}$$

To simplify V_S we are interested in eliminating this term. This yields the trivial differential constraint, $\partial_t r=-2w_2$.

Together with the assumption above, $r(t=0)=0$, it is solved by

$$r = -2\int_0^t dt' w_2(t'), \tag{5}$$

With these choices, we are left with

$$V_S = J_x a[w_1^* \cosh(J_x r) - w_1 J_x \sinh(J_x r)] + \text{H.c.} \tag{6}$$

Since V_S in Eq. (6) is linear in the mode operators, it is analytically solvable. Rotating back to the original frame, the resulting unitary evolution operator due to V_I is

$$U_I(t) = S(J_x r) D(J_x \alpha) e^{-i\{J_x^2[\Phi_2(t)+\Phi_4(t)]+J_x\Phi_3(t)\}}. \tag{7}$$

On the spin side, the evolution in Eq. (7) is composed of a global J_x rotation with angle Φ_3, and the desired qubit entangling operation, J_x^2 with phase $\Phi_2+\Phi_4$ (expressions for all Φ's are given below). On the oscillator side, it is composed of spin-dependent squeezing S and spin-dependent displacement D, with $D(\alpha)=\exp(\alpha a^\dagger - \alpha^* a)$.

Adopting the useful conventions, $\{f\}=\int_0^t dt_1 f(t_1)$ and $\{f\{g\}\}=\int_0^t dt_1 \int_0^{t_1} dt_2 f(t_1)g(t_2)$, introduced in Ref. [33], α and the Φ's are given by

$$\alpha = \{-i[w_1\cosh(r) - J_x w_1^* \sinh(r)]\}, \tag{8}$$

$$\Phi_2 = \text{Im}[\{w_1^*\cosh(r)\{w_1\cosh(r)\}\}], \tag{9}$$

$$\begin{aligned}\Phi_3 = {} & \text{Im}[\{w_1\cosh(r)\{w_1\sinh(r)\}\}] \\ & + \text{Im}[\{w_1^*\sinh(r)\{w_1^*\cosh(r)\}\}],\end{aligned} \tag{10}$$

$$\Phi_4 = \text{Im}[\{w_1\sinh(r)\{w_1^*\sinh(r)\}\}]. \tag{11}$$

Before analyzing the results in full we note that for a small w_2, the leading order contribution to the entangling phase is $\Phi_2+\Phi_4=\text{Im}[\{w_1^*\{w_1\}\}+4\{w_1\{w_2\}\{w_1^*\{w_2\}\}\}]$, such that Φ_2 scales as Ω^2 and Φ_4 as Ω^4. This dependence is different from that of the MS scheme and its generalizations, and provides the opportunity to mitigate deviations in Ω.

Using Eq. (7) we formulate constraints for the generation of two-qubit entangling gates, which are robust to deviations in Ω, and then choose the proper w's that will satisfy these constraints. We first require that at the gate time $t=T$ there will be no residual displacement or squeezing, i.e., that $r(T)=\alpha(T)=0$, and no rotation of J_x, i.e., $\Phi_3(T)=0$. Explicitly, this requires

$$\{w_1\cosh(r)\}=0, \tag{12}$$

$$\{w_1^*\sinh(r)\}=0, \tag{13}$$

$$r(t=T)=\{w_2\}=0, \tag{14}$$

$$\Phi_3(T)=0. \tag{15}$$

Crucially, Eqs. (12) and (13) are required to render the gate operation independent of the initial state of the motional mode, i.e., independent of temperature.

Next, without loss of generality we choose the entanglement phase to be $\varphi=-\pi/2$, a value that rotates the computational basis to fully entangled states:

$$\Phi_2(T)+\Phi_4(T)=\varphi=-\pi/2. \tag{16}$$

Then, robustness to errors in Ω is provided by

$$\partial_\Omega[\Phi_2(T)+\Phi_4(T)]=0. \tag{17}$$

That is, we assume a small error, $\Omega\to\Omega+\delta\Omega$, and eliminate the leading order contribution of this error to the entanglement phase. This can be generalized to next order terms. In principle, similar constraints are required also for other quantities, e.g., residual displacement. However, we show below that these are unnecessary and fulfilled by construction.

Our compiled list of six constraints does not uniquely define the drives w_1, w_2. We analyze these constraints in terms of frequencies. All the constraints are expressed as integrals from $t=0$ to $t=T$. For these integrals to vanish, the integrands must be composed of nonzero multiples of the gate rate $\xi=2\pi/T$. The choice,

$$w_1(t)=\sum_n a_{2n+1}e^{i\xi(2n+1)t}, \quad r(t)=\sum_n s_{2n}\sin(2\xi n t), \tag{18}$$

in which w_1 is made of odd harmonics of the gate rate and r of a sine series of even harmonics, guarantees that products of the form $w_1\cosh(r)$ and $w_1\sinh(r)$ will not have components at zero frequency, and will therefore integrate to zero. This choice guarantees, then, compatibility with the constraints (12)–(14). Furthermore, the choice to expand r in a sine series (and not cosine) satisfies Eq. (15) (see the Supplemental Material [53]). These considerations are independent of Ω and are therefore resilient to deviations of it.

We are left with two constraints, Eq. (16), which sets the entangling phase, and Eq. (17), which makes it robust to deviation in Ω. Appropriately, these are satisfied with two degrees of freedom. There are infinitely many solutions to these constraints. The simplest uses a_3 and s_2 (setting all other to zero). This minimal gate scheme is presented in the Supplemental Material [53].

We employ a more elaborate solution, making use of a_3, a_5, a_7, s_2, and s_4, in order to combine this new result with previously demonstrated robustness properties: mitigation of unwanted off-resonant carrier and sideband couplings, robustness to deviations in the gate time, resilience to phonon mode heating, and robustness to motional mode errors [14,18,23]. These all correspond to constraints which are linear in the a_n's and s_n's and are straightforward to implement (see the Supplemental Material [53]). Yielding,

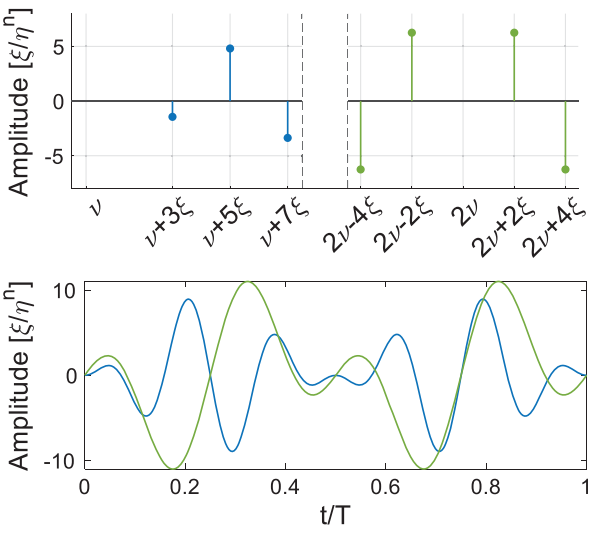

FIG. 2. Spectrum and resulting modulation used to generate our robust gate. Top: spectrum of the first (blue) and second (green) sidebands. The amplitude is given in units of ξ/η^n, with n the sideband order. Bottom: resulting time-domain modulation of the first (blue line) and second (green line) sidebands. Both modulations vanish continuously at $t = 0$ and $t = T$, thus mitigating off-resonance coupling to unwanted transitions.

$$w_1(t) = \frac{a}{3}(3e^{3i\xi t} - 10e^{5i\xi t} + 7e^{7i\xi t}), \tag{19}$$

$$r(t) = s\left[\sin(2\xi t) - \frac{1}{2}\sin(4\xi t)\right]. \tag{20}$$

Thus we still have only two undetermined degrees of freedom, a and s, required to satisfy Eqs. (16) and (17). We Taylor expand the hyperbolic functions in these constraints, yielding quadratic equations for a and s, which are solved analytically. We then optimize these solutions numerically with a straightforward gradient descent. This yields $a = 0.3608\xi$ and $s = 0.7820$, which constitutes a 3% correction to the analytical solution (see the Supplemental Material [53]).

The resulting spectrum is presented in Fig. 2 (top) showing the spectral components modulating the first (blue) and second (green) sidebands. The amplitude of the spectrum is normalized by the Lamb-Dicke parameter to the power of the sideband order; i.e., the second sideband modulation is η^{-1} times stronger than the first sideband modulation. The corresponding time-domain modulation of the sidebands due to our drive is shown in Fig. 2 (bottom). We note that both modulations continuously vanish at the start and the end of the gate, which acts to reduce off-resonance coupling to unwanted transitions [12]. The second sideband drive is significant and cannot be naively treated perturbatively [33].

The Rabi frequency Ω required by our scheme is $\Omega_{\text{robust}}/\Omega_{\text{MS}} \approx 4.8 + 6.4/\eta$, with Ω_{MS} the Rabi frequency required for a MS gate. Our gate is more demanding than

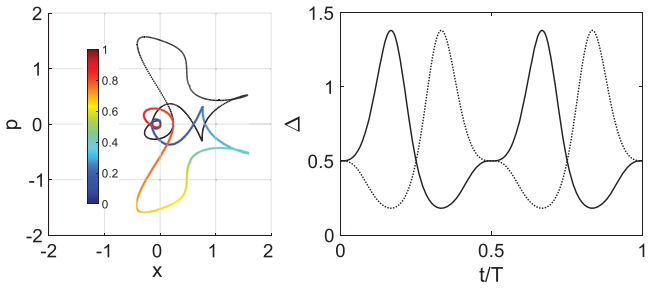

FIG. 3. Motion in phase space. Left: phase-space displacements of the $|{+}{+}\rangle$ state, with color corresponding to evolution time t/T and $|{-}{-}\rangle$ state (dashed lines). The two trajectories are related by a reflection through the $p = 0$ axis and time reversal. Right: standard deviation of position $\Delta x = \exp(r)/2$ (solid line) and momentum $\Delta p = \exp(-r)/2$ (dashed line) for the $|{+}{+}\rangle$ state, revealing oscillations of squeezing and antisqueezing in both quadratures. These are the same for momentum (solid line) and position (dashed line) in the $|{-}{-}\rangle$ state, respectively.

the MS requirements, showing that robustness is afforded at the price of additional drive power. In a typical case of two ions with a Lamb-Dicke parameter $\eta = 0.144$, a gate time of 10 μs requires total laser power of 0.8 mW in the usual MS gate and 40 mW for our fully robust gate (see the Supplemental Material [53]).

The Lamb-Dicke parameter η scales as $N^{-1/2}$, with N the number of ions in the chain. Therefore the ratio $\Omega_{\text{robust}}/\Omega_{\text{MS}}$ scales, in leading order, as $\sqrt{N}$. This implies that our method is better suited to trapped ion quantum computers where only the entangled ions are effectively trapped together, such as the quantum charge-coupled device [6,55], which has recently demonstrated remarkable results [56], or ion traps incorporating optical tweezers for mode shaping [57,58].

Nevertheless, the power requirements may be too stringent for some implementations, while the attained robustness can exceed the actual expected noise level. We mitigate this by allowing "tunability" of the robustness. Specifically, we relax constraint Eq. (17), and instead impose a constraint directly on the value of Φ_4 [still satisfying Eqs. (12)–(16)]. In leading order the fidelity of the tuned gate is

$$F \approx 1 - \frac{\pi^2}{4}\left(1 - \frac{\Phi_4}{2.24}\right)\delta\Omega^2 + \mathcal{O}(\delta\Omega^4, \Phi_4^2), \tag{21}$$

showing that the leading order contribution of $\delta\Omega$ can be completely eliminated by Φ_4, but also tuned arbitrarily. Accordingly, the tunable gate Rabi frequency now scales as

$$\Omega_{\text{tunable}}/\Omega_{\Phi_4=0} \approx 1 + 1.5\sqrt{\Phi_4}/\eta + \mathcal{O}(\eta, \Phi_4), \tag{22}$$

with $\Omega_{\Phi_4=0}$ the Rabi frequency for a gate tuned to $\Phi_4 = 0$; i.e., it is not robust to deviations in Ω. Thus the gate's robustness to deviation in driving field amplitude

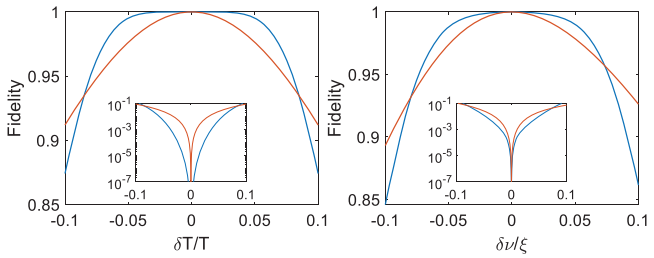

FIG. 4. Additional robustness properties of our gate (blue lines) compared to the MS gate (red lines). Insets show the same data recast as infidelity (log scale). Left: gate timing errors $\delta T/T$. Our gate shows a fourth order, wide response exhibiting high fidelity even with 5% errors. Right: motional mode frequency errors $\delta\nu/\xi$. Similarly, our gate exhibits a wide high-fidelity region.

may be tuned such that it matches the expected noise while optimizing the required laser power (see the Supplemental Material [53]).

The phase-space trajectories generated by our scheme are deduced by the squeezing $S(J_x r)$ and displacement $D(J_x\alpha)$ operators in Eq. (7). Because of the appearance of J_x in D and S, the states $|{+}{+}\rangle$ and $|{-}{-}\rangle$ follow different phase-space trajectories. This also occurs in the MS gate, however here we also have J_x operators in α, hence the trajectories are not simply reflected about the origin, as in the MS case.

The phase-space displacement of $|{+}{+}\rangle$ is presented in Fig. 3 (left, solid lines). The same evolution is shown for $|{-}{-}\rangle$ (dashed line). The trajectories are reflected through the $p = 0$ axis and time reversed. Using $r(T-t) = r(t)$ and $w_1(T-t) = w_1^*(t)$, this is readily confirmed. Squeezing by r changes the expectation value error of position and momentum, Δx and Δp, to $e^r/2$ and $e^{-r}/2$, respectively. The figure also shows the standard deviations (right) of x (solid line) and p (dashed line) for the $|{+}{+}\rangle$ state. Since r is real, the presented displacement and standard deviations completely define the phase-space motion.

The form of the evolution operator in Eq. (7), together with known phase-space identities [59], allows us to calculate the gate fidelity. Specifically, we calculate the overlap of the state generated by our gate with the ideal case, assuming the initial state is $|00\rangle$, at the motional ground state (see the Supplemental Material [53]). This is used to calculate the gate fidelity in the presence of Rabi frequency deviations $\delta\Omega$ shown in Fig. 1 (left) and in Eq. (21).

Moreover, the form of the drive in Eq. (20) ensures that our gate is robust to additional errors and noise. Indeed, Fig. 4 shows our gate fidelity in the presence of gate time deviations δT (left) and motional mode frequency errors $\delta\nu$ (right). For both of these errors our gate exhibits high fidelity (blue lines) which scales favorably compared to the MS gate (red lines).

In conclusion, we have used spin-dependent squeezing in order to propose a two-qubit entangling gate for trapped ions qubits, which is resilient to deviations in the driving field intensity. We do so by generating constraints, which can then be satisfied, with spectral consideration in an analytic fashion. Our new gate can be readily incorporated in the trapped ion quantum toolbox. Furthermore, our methods open the door to further development of useful aspects of spin-dependent squeezing.

We thank David Schwerdt for helpful discussions. This work was supported by the Israeli Science Foundation, the Israeli Ministry of Science Technology and Space, the Minerva Stiftung, the European Union's Horizon 2020 research and innovation programme (Grant Agreement LEGOTOP No. 788715), the DFG (CRC/Transregio 183, EI 519/7-1), and ISF Quantum Science and Technology (2074/19, 1376/19 and 3457/21).

[1] D. Aharonov and M. Ben-Or, Fault-tolerant quantum computation with constant error rate, SIAM J. Comput. **38**, 1207 (2008).

[2] C. D. Bruzewicz, J. Chiaverini, R. McConnell, and J. M. Sage, Trapped-ion quantum computing: Progress and challenges, Appl. Phys. Rev. **6**, 021314 (2019).

[3] M. Kjaergaard, M. E. Schwartz, J. Braumüller, P. Krantz, J. I.-J. Wang, S. Gustavsson, and W. D. Oliver, Superconducting qubits: Current state of play, Annu. Rev. Condens. Matter Phys. **11**, 369 (2020).

[4] Y. Alexeev *et al.*, Quantum computer systems for scientific discovery, PRX Quantum **2**, 017001 (2021).

[5] L. Postler, S. Heußen, I. Pogorelov, M. Rispler, T. Feldker, M. Meth, C. D. Marciniak, R. Stricker, M. Ringbauer, R. Blatt, P. Schindler, M. Müller, and T. Monz, Demonstration of fault-tolerant universal quantum gate operations, Nature (London) **605**, 675 (2022).

[6] J. M. Pino, J. M. Dreiling, C. Figgatt, J. P. Gaebler, S. A. Moses, M. Allman, C. Baldwin, M. Foss-Feig, D. Hayes, K. Mayer *et al.*, Demonstration of the trapped-ion quantum CCD computer architecture, Nature (London) **592**, 209 (2021).

[7] L. Egan, D. M. Debroy, C. Noel, A. Risinger, D. Zhu, D. Biswas, M. Newman, M. Li, K. R. Brown, M. Cetina *et al.*, Fault-tolerant control of an error-corrected qubit, Nature (London) **598**, 281 (2021).

[8] C. J. Ballance, T. P. Harty, N. M. Linke, M. A. Sepiol, and D. M. Lucas, High-Fidelity Quantum Logic Gates Using Trapped-Ion Hyperfine Qubits, Phys. Rev. Lett. **117**, 060504 (2016).

[9] J. P. Gaebler, T. R. Tan, Y. Lin, Y. Wan, R. Bowler, A. C. Keith, S. Glancy, K. Coakley, E. Knill, D. Leibfried, and D. J. Wineland, High-Fidelity Universal Gate Set for $^{9}Be^{+}$ Ion Qubits, Phys. Rev. Lett. **117**, 060505 (2016).

[10] C. R. Clark, H. N. Tinkey, B. C. Sawyer, A. M. Meier, K. A. Burkhardt, C. M. Seck, C. M. Shappert, N. D. Guise, C. E. Volin, S. D. Fallek, H. T. Hayden, W. G. Rellergert, and K. R. Brown, High-Fidelity Bell-State Preparation with $^{40}Ca^{+}$ Optical Qubits, Phys. Rev. Lett. **127**, 130505 (2021).

[11] R. Srinivas, S. C. Burd, H. M. Knaack, R. T. Sutherland, A. Kwiatkowski, S. Glancy, E. Knill, D. J. Wineland, D. Leibfried, A. C. Wilson, D. T. C. Allcock, and

D. H. Slichter, High-fidelity laser-free universal control of trapped ion qubits, Nature (London) **597**, 209 (2021).
[12] C. F. Roos, Ion trap quantum gates with amplitude-modulated laser beams, New J. Phys. **10**, 013002 (2008).
[13] T. J. Green and M. J. Biercuk, Phase-Modulated Decoupling and Error Suppression in Qubit-Oscillator Systems, Phys. Rev. Lett. **114**, 120502 (2015).
[14] F. Haddadfarshi and F. Mintert, High fidelity quantum gates of trapped ions in the presence of motional heating, New J. Phys. **18**, 123007 (2016).
[15] T. Manovitz, A. Rotem, R. Shaniv, I. Cohen, Y. Shapira, N. Akerman, A. Retzker, and R. Ozeri, Fast Dynamical Decoupling of the Mølmer-Sørensen Entangling Gate, Phys. Rev. Lett. **119**, 220505 (2017).
[16] M. Palmero, S. Martínez-Garaot, D. Leibfried, D. J. Wineland, and J. G. Muga, Fast phase gates with trapped ions, Phys. Rev. A **95**, 022328 (2017).
[17] J. D. Wong-Campos, S. A. Moses, K. G. Johnson, and C. Monroe, Demonstration of Two-Atom Entanglement with Ultrafast Optical Pulses, Phys. Rev. Lett. **119**, 230501 (2017).
[18] Y. Shapira, R. Shaniv, T. Manovitz, N. Akerman, and R. Ozeri, Robust Entanglement Gates for Trapped-Ion Qubits, Phys. Rev. Lett. **121**, 180502 (2018).
[19] G. Zarantonello, H. Hahn, J. Morgner, M. Schulte, A. Bautista-Salvador, R. F. Werner, K. Hammerer, and C. Ospelkaus, Robust and Resource-Efficient Microwave Near-Field Entangling $^{9}Be^{+}$ Gate, Phys. Rev. Lett. **123**, 260503 (2019).
[20] P. H. Leung, K. A. Landsman, C. Figgatt, N. M. Linke, C. Monroe, and K. R. Brown, Robust 2-Qubit Gates in a Linear Ion Crystal Using a Frequency-Modulated Driving Force, Phys. Rev. Lett. **120**, 020501 (2018).
[21] P. H. Leung and K. R. Brown, Entangling an arbitrary pair of qubits in a long ion crystal, Phys. Rev. A **98**, 032318 (2018).
[22] V. M. Schäfer, C. J. Ballance, K. Thirumalai, L. J. Stephenson, T. G. Ballance, A. M. Steane, and D. M. Lucas, Fast quantum logic gates with trapped-ion qubits, Nature (London) **555**, 75 (2018).
[23] A. E. Webb, S. C. Webster, S. Collingbourne, D. Bretaud, A. M. Lawrence, S. Weidt, F. Mintert, and W. K. Hensinger, Resilient Entangling Gates for Trapped Ions, Phys. Rev. Lett. **121**, 180501 (2018).
[24] R. T. Sutherland, R. Srinivas, S. C. Burd, D. Leibfried, A. C. Wilson, D. J. Wineland, D. T. C. Allcock, D. H. Slichter, and S. B. Libby, Versatile laser-free trapped-ion entangling gates, New J. Phys. **21**, 033033 (2019).
[25] C. Figgatt, A. Ostrander, N. M. Linke, K. A. Landsman, D. Zhu, D. Maslov, and C. Monroe, Parallel entangling operations on a universal ion-trap quantum computer, Nature (London) **572**, 368 (2019).
[26] Y. Lu, S. Zhang, K. Zhang, W. Chen, Y. Shen, J. Zhang, J.-N. Zhang, and K. Kim, Global entangling gates on arbitrary ion qubits, Nature (London) **572**, 363 (2019).
[27] Y. Shapira, R. Shaniv, T. Manovitz, N. Akerman, L. Peleg, L. Gazit, R. Ozeri, and A. Stern, Theory of robust multiqubit nonadiabatic gates for trapped ions, Phys. Rev. A **101**, 032330 (2020).
[28] R. T. Sutherland, R. Srinivas, S. C. Burd, H. M. Knaack, A. C. Wilson, D. J. Wineland, D. Leibfried, D. T. C. Allcock, D. H. Slichter, and S. B. Libby, Laser-free trapped-ion entangling gates with simultaneous insensitivity to qubit and motional decoherence, Phys. Rev. A **101**, 042334 (2020).
[29] J. Lishman and F. Mintert, Trapped-ion entangling gates robust against qubit frequency errors, Phys. Rev. Res. **2**, 033117 (2020).
[30] Y. Wang, J.-L. Wu, J.-X. Han, Y.-Y. Jiang, Y. Xia, and J. Song, Noise-resistant phase gates with amplitude modulation, Phys. Rev. A **102**, 032601 (2020).
[31] A. R. Milne, C. L. Edmunds, C. Hempel, F. Roy, S. Mavadia, and M. J. Biercuk, Phase-Modulated Entangling Gates Robust to Static and Time-Varying Errors, Phys. Rev. Appl. **13**, 024022 (2020).
[32] C. D. B. Bentley, H. Ball, M. J. Biercuk, A. R. R. Carvalho, M. R. Hush, and H. J. Slatyer, Numeric optimization for configurable, parallel, error-robust entangling gates in large ion registers, Adv. Quantum Technol. **3**, 2000044 (2020).
[33] M. Sameti, J. Lishman, and F. Mintert, Strong-coupling quantum logic of trapped ions, Phys. Rev. A **103**, 052603 (2021).
[34] M. Duwe, G. Zarantonello, N. Pulido-Mateo, H. Mendpara, L. Krinner, A. Bautista-Salvador, N. V. Vitanov, K. Hammerer, R. F. Werner, and C. Ospelkaus, Numerical optimization of amplitude-modulated pulses in microwave-driven entanglement generation (2022).
[35] M. Kang, Q. Liang, B. Zhang, S. Huang, Y. Wang, C. Fang, J. Kim, and K. R. Brown, Batch Optimization of Frequency-Modulated Pulses for Robust Two-Qubit Gates in Ion Chains, Phys. Rev. Appl. **16**, 024039 (2021).
[36] R. Blümel, N. Grzesiak, N. Pisenti, K. Wright, and Y. Nam, Power-optimal, stabilized entangling gate between trapped-ion qubits, npj Quantum Inf. **7**, 147 (2021).
[37] R. Blümel, N. Grzesiak, N. H. Nguyen, A. M. Green, M. Li, A. Maksymov, N. M. Linke, and Y. Nam, Efficient Stabilized Two-Qubit Gates on a Trapped-Ion Quantum Computer, Phys. Rev. Lett. **126**, 220503 (2021).
[38] L. Dong, I. n. Arrazola, X. Chen, and J. Casanova, Phase-Adaptive Dynamical Decoupling Methods for Robust Spin-Spin Dynamics in Trapped Ions, Phys. Rev. Appl. **15**, 034055 (2021).
[39] C. H. Valahu, A. M. Lawrence, S. Weidt, and W. K. Hensinger, Robust entanglement by continuous dynamical decoupling of the j-coupling interaction, New J. Phys. **23**, 113012 (2021).
[40] K. Wang, J.-F. Yu, P. Wang, C. Luan, J.-N. Zhang, and K. Kim, Ultra-fast multi-qubit global-entangling gates without individual addressing of trapped ions, arXiv:2201.06959.
[41] T. Manovitz, Y. Shapira, L. Gazit, N. Akerman, and R. Ozeri, Trapped-ion quantum computer with robust entangling gates and quantum coherent feedback, PRX Quantum **3**, 010347 (2022).
[42] C. Fang, Y. Wang, S. Huang, K. R. Brown, and J. Kim, Crosstalk Suppression in Individually Addressed Two-Qubit Gates in a Trapped-Ion Quantum Computer, Phys. Rev. Lett. **129**, 240504 (2022).
[43] C. H. Valahu, I. Apostolatos, S. Weidt, and W. K. Hensinger, Quantum control methods for robust entanglement of trapped ions, J. Phys. B **55**, 204003 (2022).

[44] A. Sørensen and K. Mølmer, Quantum Computation with Ions in Thermal Motion, Phys. Rev. Lett. **82**, 1971 (1999).
[45] A. Sørensen and K. Mølmer, Entanglement and quantum computation with ions in thermal motion, Phys. Rev. A **62**, 022311 (2000).
[46] K. R. Brown, J. Kim, and C. Monroe, Co-designing a scalable quantum computer with trapped atomic ions, npj Quantum Inf. **2**, 16034 (2016).
[47] E. Mount, D. Gaultney, G. Vrijsen, M. Adams, S.-Y. Baek, K. Hudek, L. Isabella, S. Crain, A. van Rynbach, P. Maunz, and J. Kim, Scalable digital hardware for a trapped ion quantum computer, Quantum Inf. Process. **15**, 5281 (2016).
[48] B. Andrade, Z. Davoudi, T. Graß, M. Hafezi, G. Pagano, and A. Seif, Engineering an effective three-spin Hamiltonian in trapped-ion systems for applications in quantum simulation, Quantum Sci. Technol. **7**, 034001 (2022).
[49] O. Katz, M. Cetina, and C. Monroe, *n*-Body Interactions between Trapped Ion Qubits via Spin-Dependent Squeezing, Phys. Rev. Lett. **129**, 063603 (2022).
[50] Y. Wang, S. Crain, C. Fang, B. Zhang, S. Huang, Q. Liang, P. H. Leung, K. R. Brown, and J. Kim, High-Fidelity Two-Qubit Gates Using a Microelectromechanical-System-Based Beam Steering System for Individual Qubit Addressing, Phys. Rev. Lett. **125**, 150505 (2020).
[51] D. J. Wineland, C. Monroe, W. M. Itano, D. Leibfried, B. E. King, and D. M. Meekhof, Experimental issues in coherent quantum-state manipulation of trapped atomic ions, J. Res. Natl. Inst. Stand. Technol. **103**, 259 (1998).
[52] G. Harari, Y. Ben-Aryeh, and A. Mann, Propagator for the general time-dependent harmonic oscillator with application to an ion trap, Phys. Rev. A **84**, 062104 (2011).
[53] See Supplemental Material at http://link.aps.org/supplemental/10.1103/PhysRevLett.130.030602 for additional derivation details, which includes Ref. [54].
[54] R. Ozeri, W. M. Itano, R. B. Blakestad, J. Britton, J. Chiaverini, J. D. Jost, C. Langer, D. Leibfried, R. Reichle, S. Seidelin, J. H. Wesenberg, and D. J. Wineland, Errors in trapped-ion quantum gates due to spontaneous photon scattering, Phys. Rev. A **75**, 042329 (2007).
[55] D. Kielpinski, C. Monroe, and D. J. Wineland, Architecture for a large-scale ion-trap quantum computer, Nature (London) **417**, 709 (2002).
[56] C. Ryan-Anderson *et al.*, Implementing fault-tolerant entangling gates on the five-qubit code and the color code, arXiv:2208.01863.
[57] Y. H. Teoh, M. Sajjan, Z. Sun, F. Rajabi, and R. Islam, Manipulating phonons of a trapped-ion system using optical tweezers, Phys. Rev. A **104**, 022420 (2021).
[58] M. Mazzanti, R. X. Schüssler, J. D. Arias Espinoza, Z. Wu, R. Gerritsma, and A. Safavi-Naini, Trapped Ion Quantum Computing Using Optical Tweezers and Electric Fields, Phys. Rev. Lett. **127**, 260502 (2021).
[59] C. Gerry and P. Knight, *Introductory Quantum Optics* (Cambridge University Press, Cambridge, England, 2004).